Available online at www.sciencedirect.com
ScienceDirect
Journal of Catalysis 250 (2007) 240–246
JOURNAL OF CATALYSIS
www.elsevier.com/locate/jcat

Mechanism of ammonia oxidation over oxides studied by temporal analysis of products

Javier Pérez-Ramírez [a,b,*], Evgenii V. Kondratenko [c,*]

[a] *Institute of Chemical Research of Catalonia (ICIQ), Av. Països Catalans 16, 43007 Tarragona, Spain*
[b] *Catalan Institution for Research and Advanced Studies (ICREA), Pg. Lluís Companys 23, 08010 Barcelona, Spain*
[c] *Leibniz-Institut für Katalyse e.V. an der Universität Rostock, Aussenstelle Berlin, Richard-Willstätter-Str. 12, 12489 Berlin, Germany*

Received 9 April 2007; revised 11 June 2007; accepted 12 June 2007

Available online 30 July 2007

Abstract

A temporal analysis of products (TAP) reactor was used to study the mechanism of ammonia oxidation at high temperature (1073 K) over Fe_2O_3, Cr_2O_3, and CeO_2. The results were compared with those obtained over the industrially applied Pt_{95}–Rh_5 alloy. Analysis of characteristic times of the transient responses of N_2 and NO made it possible to gain insight into the sequence of their formation. A common feature of both metal oxide and noble metal catalysts is that NO is a primary product of NH_3 oxidation, whereas N_2 results mainly from secondary transformations of NO. The amount of N_2O formed over the oxides was minimal. Multipulse NH_3 experiments in the absence of gas-phase O_2 give unequivocal evidence of the participation of surface lattice oxygen of the metal oxides in the reaction of NH_3 to NO. The degree of reduction of the oxide surface determines the product distribution but does not alter the catalytic activity for NH_3 conversion. Greater reduction favors the reaction channel to N_2 over that to NO. The desired reaction follows a Mars–van Krevelen-type scheme involving the participation of lattice oxygen in the NH_3 conversion to NO and regeneration of the so-formed vacancies by gas-phase O_2 and bulk lattice oxygen. Replenishment of surface vacancies by the diffusion of bulk oxygen occurs to a significant extent over Fe_2O_3. However, when NH_3 and O_2 are fed together, dissociative adsorption of gas-phase oxygen can be considered the main mechanism for vacancy regeneration.

Keywords: Ammonia oxidation; High-temperature catalysis; Oxides; Noble metal alloys; Mars–van Krevelen scheme; Temporal analysis of products; TAP reactor

1. Introduction

Nitric acid producers traditionally rely on platinum group metal (PGM) alloy gauzes as catalysts for the high-temperature ammonia oxidation. This is because PGMs display NO selectivities of 94–96% and stable performance in campaigns ranging from 3 to 12 months [1]. But the PGM technology has some significant drawbacks, including high production cost and metal loss in the form of volatile oxides. Moreover, nitric acid production is the largest source of N_2O in the chemical industry, and implementation of abatement technology is being enforced [2]. The aforementioned issues have stimulated research into replacing noble metals by transition metal oxides for ammonia oxidation.

The search for oxide-based materials (OBMs) began at the beginning of the twentieth century and has produced numerous patent applications over the decades. Claimed catalytic materials include mixed oxides with spinel, perovskite, and K_2NiF_4-type structures preferably containing Co, Fe, Mn, Ni, Bi, or Cr, and various mixtures thereof [2–5]. However, attempts to replace PGM gauzes by OBM in the form of particles, pellets, or monoliths have failed due to insufficient NO selectivity and rapid catalyst deactivation. Consequently, direct extrapolation of optimal process conditions for PGM to OBM systems has proven ineffectual.

To rationally develop a process for NH_3 oxidation to NO catalyzed by OBM, a solid understanding of the reaction mechanism and kinetics is of prime importance. Extensive

* Corresponding authors. Fax: +34 977 920 224.
E-mail addresses: jperez@iciq.es (J. Pérez-Ramírez), evgenii.kondratenko@catalysis.de (E.V. Kondratenko).

0021-9517/$ – see front matter
doi:10.1016/j.jcat.2007.06.014

fundamental studies have been carried out over Pt single crystals, foils, wires, and support systems using batch and flow reactors at ambient pressure, as well as surface science techniques with molecular beams under ultra-high vacuum (UHV) [6–12]. In contrast, mechanistic investigations of high-temperature ammonia oxidation (>1000 K) over oxide catalysts have not been reported to date. Previous studies by Trifirò and Pasquon [13], Griffiths et al. [14], Il'chenko and Golodets [15,16], Sil'chenkova et al. [17], and Slavinskaya et al. [18] are restricted to the low-temperature regime (<873 K), where N_2 and/or N_2O are the main reaction products. Studies on metal oxides have concluded that the strength of the metal-terminal oxygen bond is crucial in determining the product distribution in ammonia oxidation over oxides in the low-temperature and high-temperature regimes [3,13,16]. The often-used steady-state approaches lack sufficient time resolution to provide detailed insight into the reaction mechanism. This is aggravated at high temperature, where the lifetime of reaction intermediates is extremely short due to high reaction rates. A reactive molecular beam study of the ammonia oxidation over oxide single crystals has not been published to date. Presumably, this is due to the high complexity of specimen preparation compared with pure metal surfaces, as well as to the extensive reduction of the catalyst surface under UHV conditions.

Herein we present the first experimental study exploring the mechanism of the high-temperature ammonia oxidation over Fe_2O_3, Cr_2O_3, and CeO_2. This study investigated the origins of the reaction products, as well as the nature and amount of active and selective oxygen species for the reaction to NO and N_2. In light of this, mechanistic differences and similarities between oxides and noble metal alloys are established. For this purpose, we used the temporal analysis of products (TAP) reactor, a transient pulse technique operating in vacuum with submillisecond time resolution [19,20]. As we reported previously [21–24], the intrinsic characteristics of the TAP reactor made it possible to investigate the high-temperature ammonia oxidation (1073–1173 K) over commercial PGM gauzes under isothermal conditions, a key aspect in this highly exothermic process. Moreover, peak pressures can be up to 10^9 times higher than in typical UHV studies. This feature is crucial for minimizing the degree of surface reduction in metal oxides and ultimately narrowing the pressure gap with respect to ambient pressure studies.

2. Experimental

The mechanism of ammonia oxidation was investigated over Fe_2O_3 (Aldrich, 99.98%), Cr_2O_3 (Aldrich, 99.9%), CeO_2 (Aldrich, 99.995%), and Pt_{95}–Rh_5 alloy (K.A. Rasmussen, woven gauze, 1024 mesh per cm^2, wire diameter 76 μm). A detailed description of the TAP-2 reactor for investigating NH_3–O_2 and NH_3–NO interactions over PGM gauzes has been given elsewhere [22,23]. Approximately 25 mg of oxide particles (sieve fraction, 250–350 μm) were sandwiched between two layers of quartz particles of the same size fraction and positioned in the isothermal zone of a quartz microreactor (6 mm i.d., 40 mm long). Before the transient experiments, the sample was pretreated in flowing pure O_2 at 1073 K and ambient pressure for 2 h. Afterward, the microreactor was evacuated at 1073 K to 10^{-5} Pa, and the catalyst was subjected to pulses of oxygen (a total of ca. 1 μmol O_2) at the reaction temperature (1073 K). Subsequently, pulses containing a small amount of the reactants (10^{16} molecules per pulse) diluted by an inert gas were injected in the reactor through one or two high-speed valves. The pulse size lays on the molecular diffusion regime of reactants and products along the reactor. As we showed in our previous study on ammonia oxidation over PGM, using relatively large pulse sizes was vital for elucidating the mechanism of N_2O formation [22]. This was not possible when typical pulse sizes in the Knudsen regime (10^{14} molecules per pulse) were applied.

Three types of transient experiments were performed in this work: (1) multipulses of ammonia (NH_3:Ne = 1:1), (2) single pulses of NH_3:O_2:Ne = 1:2:1 or $^{15}NH_3$:NO:Ne = 1:1:1 mixtures, and (3) sequential pulses of oxygen (O_2:Xe = 1:1) and ammonia (NH_3:Ne = 1:1) at time delays (Δt) in the range of 0.1–2 s. The latter are called "pump-probe" experiments. To ensure quantification of pump-probe experiments, reaction mixtures with different inert gases were used; otherwise, the transient responses of the same inert gas (used as an internal standard) in the two pulses would be overlapped. Xe (4.0), Ne (4.5), O_2 (4.6), NH_3 (2.5), NO (2.5), and $^{15}NH_3$ (99.9% atoms of ^{15}N, ISOTEC) were used without additional purification. Transient responses were monitored at atomic mass units (amus) related to reactants, products, and inert gases at the reactor outlet using a quadrupole mass spectrometer (HAL RC 301, Hiden Analytical). The following amus were analyzed: 132 (Xe), 46 ($^{15}N^{15}NO$, NO_2), 45 ($^{15}N^{14}NO$), 44 ($^{14}N^{14}NO$), 32 (O_2), 31 ($H^{14}NO$, ^{15}NO), 30 (^{14}NO, $^{15}N^{15}N$, $^{15}N^{15}NO$, $^{14}N^{14}NO$), 29 ($^{15}N^{14}N$, $^{15}N^{14}NO$), 28 ($^{14}N^{14}NO$, $^{14}N^{14}N$), 20 (Ne), 18 (H_2O, $^{15}NH_3$), 17 ($^{14}NH_3$, $^{15}NH_3$, H_2O, OH), 15 ($^{14}NH_3$), and 2 (H_2). If not specified, the label N in nitrogen-containing compounds along the manuscript corresponds to the most abundant ^{14}N isotope. For each amu, pulses were repeated 10 times and averaged to improve the signal-to-noise ratio. In multipulse experiments with ammonia, individual transient responses were recorded without averaging. The concentration of feed components and reaction products was determined from the respective amus using standard fragmentation patterns and sensitivity factors.

3. Results and discussion

3.1. Origin of products in ammonia oxidation

Fig. 1 compares the transient responses of O_2, NO, and N_2 resulting from sequential pulsing of oxygen and ammonia at $\Delta t = 0.5$ s over the catalysts. The transients at other time delays in the range of $\Delta t = 0.1$–2 s were qualitatively very similar to those given in Fig. 1 and are not shown for conciseness. Each response has a characteristic residence time, temporal maximum, and decay. The sharp decrease of the O_2 response (dashed line) on NH_3 pulsing (at $t = 0.5$ s in Fig. 1) is indicative of the

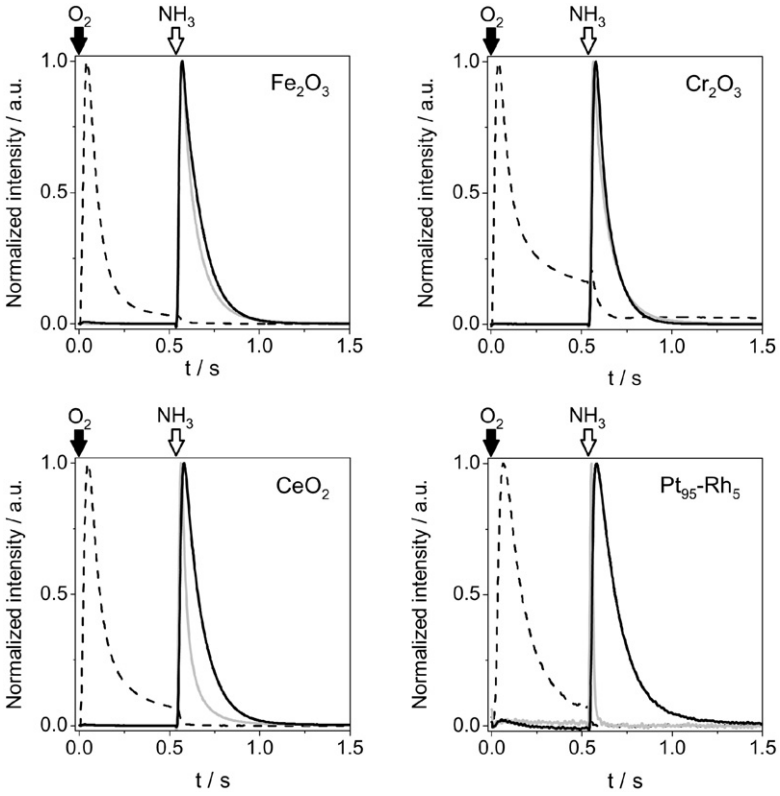

Fig. 1. Normalized transient responses of O_2 (dashed black line), NO (solid gray line), and N_2 (solid black line) over the catalysts during sequential pulsing of O_2:Xe = 1:1 and NH_3:Ne = 1:1 with $\Delta t = 0.5$ s at 1073 K. Pulse size of O_2 and $NH_3 \sim 10^{16}$ molecules.

rapid reaction of surface oxygen species with ammonia. The responses of NO and N_2 (gray and black solid lines, respectively), which were detected only in the NH_3 pulse, have very similar shapes over Fe_2O_3 and Cr_2O_3. However, the NO response over CeO_2 and Pt_{95}–Rh_5 gauze was much sharper than the N_2 response. Only a minimal amount of N_2O was formed over the oxides, practically within the detection limit of the mass spectrometer. This can be tentatively attributed to the capability of metal oxide catalysts for N_2O decomposition at high temperature [2]. Based on this, the analysis of reaction products reported below concentrates on NO and N_2.

Insights into the sequence of product formation in ammonia oxidation over the catalysts were obtained by analyzing the time of maximum transient response (t_{max}) and the width at the half-height of the intensity-normalized response ($t_{h/2}$). These characteristic times were determined in the transients of NO and N_2 and are displayed in Fig. 2. The error in these values is estimated at ±0.001 s due to the sub-millisecond resolution of the TAP technique. The t_{max} and $t_{h/2}$ values of NO are consistently lower than those of N_2. The characteristic times of the NO response vary significantly in the catalytic materials investigated (t_{max} of 0.552–0.567 s and $t_{h/2}$ of 0.018–0.074 s), in contrast to the narrower variation of the values in the N_2 response (t_{max} of 0.572–0.580 s and $t_{h/2}$ of 0.077–0.133 s). The marked dependence of the t_{max} and $t_{h/2}$ of NO on the catalyst composition strongly suggests the oxides' differing capabilities for production and further transformation of NO. The difference $t_{h/2}(N_2) - t_{h/2}(NO)$ increases in the order $Fe_2O_3 \sim Cr_2O_3 > CeO_2 > Pt_{95}$–$Rh_5$. Exactly the same trend

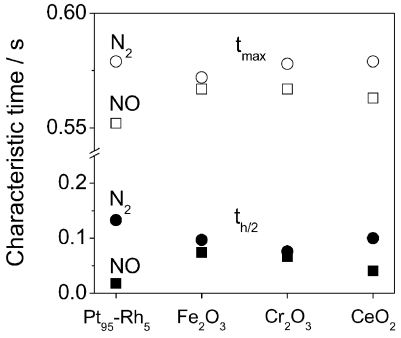

Fig. 2. Characteristic times of the transient responses of N_2 (circles) and NO (squares) over the catalysts upon sequential pulsing of oxygen and ammonia. Conditions as in caption of Fig. 1.

applies to the difference $t_{max}(N_2) - t_{max}(NO)$. In parallel with the reaction over PGM gauzes [22], the relative order of appearance (t_{max}) of NO and N_2 and the shapes ($t_{h/2}$) of NO and N_2 transient responses suggest that NO is a primary product of NH_3 oxidation, whereas the major part of N_2 is formed through secondary transformations of NO.

The secondary nature of N_2 formation over the catalysts is supported by analysis of the NO selectivity at different time delays between the O_2 and NH_3 pulses (Fig. 3, right). Simultaneous pulsing of NH_3 and O_2 mixtures (equivalent to $\Delta t = 0$ s) yielded NO selectivities in the range of 80–90%. This selectivity value remained practically unchanged over Fe_2O_3 and Cr_2O_3 upon separating the oxygen and ammonia pulses; however, the NO selectivity over Pt_{95}–Rh_5 alloy dropped to zero

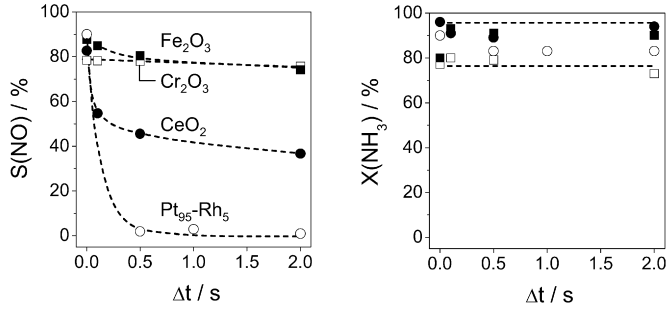

Fig. 3. NO selectivity and NH_3 conversion over the catalysts versus the time delay during sequential pulsing of O_2:Xe = 1:1 and NH_3:Ne = 1:1 at 1073 K. Pulse size as in caption of Fig. 1.

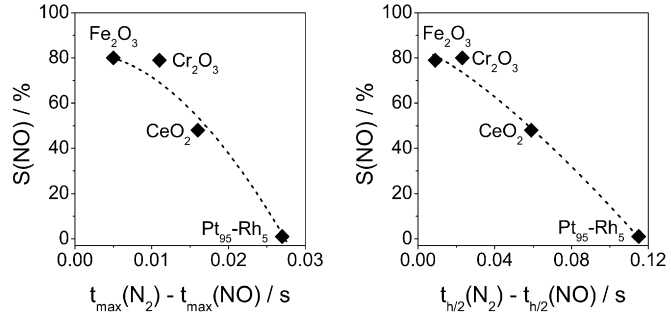

Fig. 4. NO selectivity vs the difference in the t_{max} and $t_{h/2}$ of N_2 and NO during sequential pulsing of oxygen and ammonia. Conditions as in caption of Fig. 1.

when $\Delta t \geqslant 0.5$ s. CeO_2 exhibited an intermediate behavior and NO selectivity decreased progressively with increasing time delay, with S(NO) = 40% at $\Delta t = 2$ s. A valuable correlation can be made between NO selectivity and the difference in the characteristic times of the N_2 and NO transient responses obtained in pump-probe experiments with O_2 and NH_3 at $\Delta t = 0.5$ s. As show in Fig. 4, a higher NO selectivity is attained when the differences $t_{max}(N_2) - t_{max}(NO)$ and $t_{h/2}(N_2) - t_{h/2}(NO)$ decrease. This can be understood by assuming that N_2 is partially formed through secondary transformations of NO. For Fe_2O_3 and Cr_2O_3, the NO selectivity was >80%. This means that only a small part of the NO was further converted to N_2. Consequently, the differences $t_{max}(N_2) - t_{max}(NO)$ and $t_{h/2}(N_2) - t_{h/2}(NO)$ are very low. As the catalyst's ability for secondary NO transformations increases, the NO selectivity will obviously decrease and the differences between the characteristic times of the N_2 and NO transients will become more significant.

The importance of secondary transformations of NO in ammonia oxidation (leading to N_2) was assessed by pulsing a mixture of $^{15}NH_3$ and NO over the catalysts. Application of isotopic traces is essential to determine from which reactant (ammonia and/or nitric oxide) N_2 originates. In agreement with earlier results of NH_3–NO interactions over PGM gauzes [23,24], N-containing products formed over the oxides were molecular nitrogen of varying isotopic compositions (i.e., $^{14}N^{15}N$ and $^{14}N^{14}N$), as well as isotopically labeled nitric oxide (^{15}NO). From these results, it can be posited that general mechanistic aspects of the origin of NO and N_2 during O_2–NH_3 and NH_3–

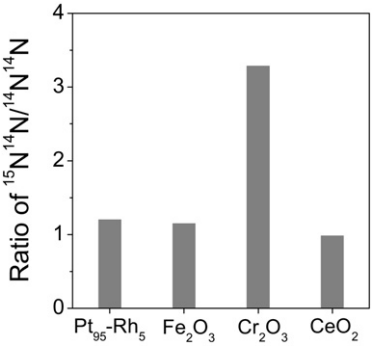

Fig. 5. Ratio of $^{15}N^{14}N$-to-$^{14}N^{14}N$ over the catalysts determined by pulsing of $^{15}NH_3$:NO:Ne = 1:1:1. Pulse size of Ne ~ 10^{16} molecules.

NO interactions are similar for PGM and oxide catalysts. Fig. 5 displays the ratio between the molar fractions of $^{15}N^{14}N$ to $^{14}N^{14}N$ over the oxide catalysts and the Pt_{95}–Rh_5 gauze. This ratio provides an indication of the catalyst's capability for N_2 formation through the NH_3–NO coupling reaction, leading to $^{15}N^{14}N$ [Eq. (1)] relative to pathways originating $^{14}N^{14}N$, that is, direct NO decomposition [Eq. (2)] and NH_3-assisted NO reduction [Eq. (3)]:

$$\text{s-}^{15}NH_x + \text{s-}^{14}NO \rightarrow {}^{15}N\,{}^{14}N + \text{s-}H_xO + \text{s}, \quad (1)$$

$$2\,{}^{14}NO + 2\text{s} \rightarrow {}^{14}N\,{}^{14}N + 2\text{s-O}, \quad (2)$$

$$2\text{s-}{}^{14}NO + \text{s-}{}^{15}NH_x \rightarrow {}^{14}N_2 + \text{s-}H_xO + \text{s-}{}^{15}N + \text{s-O}. \quad (3)$$

In these reactions, "s" represents an active site in the catalyst and the value of x can be 0, 1, or 2. As shown in Fig. 5, the ratio of $^{15}N^{14}N/^{14}N^{14}N$ is close to 1 for Pt_{95}–Rh_5, Fe_2O_3, and CeO_2 and 3.2 for Cr_2O_3. It is obvious that relative contributions of the paths shown in Eqs. (1)–(3) toward N_2 formation are influenced by the NH_3/NO ratio. Moreover, we have previously reported that for Pt_{95}–Rh_5, NO transformations to N_2 according to Eqs. (2) and (3) are suppressed more strongly in the presence of gas-phase O_2 than the NO–NH_3 coupling reaction in Eq. (1) [24]. Taking the aforementioned similarities between the noble metal gauze and oxide catalysts into account, we put forward that the reaction in Eq. (1) is the main source of N_2 when O_2 and NH_3 are fed together. The formation of $^{15}N^{15}N$ during $^{15}NH_3$–NO interactions was strongly inhibited. This observation agrees with earlier results over Pt_{95}–Rh_5 gauze [24] and indicates that significant primary formation of N_2 from NH_3 decomposition did not occur under these conditions. However, we should point out that due to an overlap of the mass spectra of NO and $^{15}N^{15}N$, very low amounts of $^{15}N^{15}N$ could not be monitored precisely.

The pump-probe experiments shown in Fig. 1 and quantified in Fig. 3 make it possible to analyze the influence of the lifetime of the oxygen species deposited in the O_2 pulse (pump) on their reactivity with NH_3 (probe). Despite the markedly different dependencies of the NO selectivity versus the time delay over the catalysts (Fig. 3, left), the NH_3 conversion varied within a narrow range (80–95%) (Fig. 3, right). This indicates that the time delay between the oxygen and ammonia pulses influenced the product distribution (NO vs N_2) but not the catalyst ability to activate NH_3. The decay in NO selectivity over the Pt_{95}–Rh_5

gauze was partly associated with the influence of the lifetime of oxygen species generated in the O_2 pulse on the selectivity [22]. Very short time delays are sufficient to decrease the coverage of short-lived oxygen species leading to NO, by either its desorption as O_2 and/or its transformation into strongly bound oxygen. The latter species can efficiently activate the ammonia molecule, explaining the unchanged NH_3 conversion, but lead to N_2. The stable NO selectivity over Cr_2O_3 and Fe_2O_3 at different time delays may indicate a longer lifetime and/or a higher concentration of surface O species capable of producing NO.

3.2. Participation of lattice oxygen in NO production

Of course, oxides contain oxygen in their lattice, in contrast to noble metal catalysts. But is this oxygen active for NH_3 conversion and subsequent NO production? To shed light on this key mechanistic aspect, multipulse experiments with ammonia were performed in the absence of gas-phase oxygen. The number of NH_3 molecules per pulse (10^{16} molecules) was two orders of magnitude lower than the total number for surface oxygen atoms (O_s) in the samples loaded in the TAP microreactor. This made it possible to accurately probe reactive lattice oxygen species in the catalysts by ammonia. The value of O_s was estimated taking into account the specific surface area of the samples measured by N_2 adsorption at 77 K (ca. 3–10 $m^2\,g^{-1}$) and the number of oxygen atoms on the surface of the most stable crystallographic planes for each oxide. The ratio of surface oxygen atoms (O_s) to the total number of oxygen atoms (O_t, determined by chemical composition analyses) in the samples was ca. 10^{-3}. The estimation of O_s is subject to a number of assumptions, because we have a polycrystalline sample and possible defect sites are not accounted for. Thus, the value of surface oxygen atoms should not be taken on a purely quantitative basis. Despite this drawback, valuable information can be obtained on the amount of oxygen species participating in ammonia oxidation depending on the oxide (vide infra).

Multipulses of NH_3 yielded no NO over Pt_{95}–Rh_5 alloy, because PGM catalysts require high coverage by short-lived O species. This situation is realized when O_2 and NH_3 are pulsed simultaneously into the TAP microreactor [22]. In contrast, the observation of NO on NH_3 multipulsing over oxide catalysts (Fig. 6) revealed the active and selective nature of surface lattice oxygen in high-temperature ammonia oxidation. The evolution of NO selectivity with the number of NH_3 pulses depends on the nature of the oxide. Cr_2O_3 and CeO_2 lose their capability for NO production after a few pulses of ammonia [S(NO) ∼ 1% after ca. 20 pulses of NH_3], whereas the decay in NO selectivity over Fe_2O_3 is significantly slower [S(NO) = 50% after 400 pulses of NH_3]. It must be stressed that the ammonia conversion was practically constant with the pulse number over the metal oxides investigated. As can be concluded from pump-probe experiments shown in Fig. 3, the pulse number does not alter the activity of the catalyst for NH_3 conversion but favors reaction channels toward N_2 formation. The decreased NO formation with the NH_3 pulse number over Cr_2O_3 and CeO_2 is accompanied by production of H_2 (Fig. 6). The high initial production of NO is related to the presence of highly reactive and

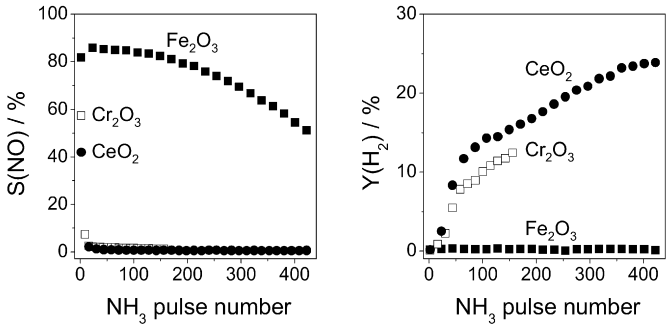

Fig. 6. NO selectivity and H_2 yield over the catalysts versus the number of pulses in multipulse experiments with NH_3 at 1073 K. Pulse size of NH_3 ∼ 10^{16} molecules.

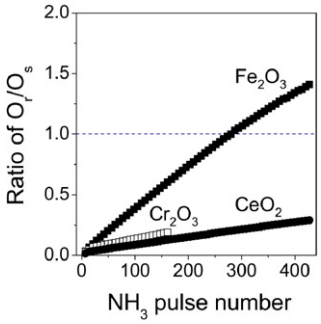

Fig. 7. Ratio of the oxygen reacted (O_r) to the initial surface oxygen (O_s) in the catalysts versus the NH_3 pulse number at 1073 K. Pulse size of NH_3 ∼ 10^{16} molecules.

selective surface lattice oxygen species. The concentration of this oxygen rapidly decreases with the NH_3 pulse number due to its removal for ammonia oxidation to NO and H_2O. Consequently, the reduced catalyst surface contains mainly strongly bound lattice oxygen species, which can activate the N–H bond in ammonia to form NH_x intermediates but are not transferable to produce gas-phase NO and H_2O. Instead, the highly reactive NH_x fragments recombine, yielding N_2 and H_2. Accordingly, in the absence of O_2 and NO in the feed pulses, primary N_2 formation through ammonia decomposition occurs over cerium and chromium oxides. Under these conditions, a similar reaction pathway also has been reported for NH_3 oxidation over PGM gauzes [22].

To gain insight into the effect of surface reduction on the product distribution of ammonia oxidation over the oxides, the ratio of reacted oxygen (O_r) to the previously estimated amount of surface oxygen species in the original sample (O_s) was plotted as a function of the number of NH_3 pulses (Fig. 7). The amount of reacted oxygen leading to NO and H_2O was determined from the amounts of NO and N_2 formed, considering the stoichiometry of the following reaction pathways:

$$NH_3 + 2.5O_{lattice} \rightarrow NO + 1.5H_2O \quad (4)$$

and

$$2NH_3 + 3O_{lattice} \rightarrow N_2 + 3H_2O. \quad (5)$$

It should be stressed that the oxygen involved in N_2 formation was calculated only from pulses in which no H_2 is produced. Because NO formation over CeO_2 and Cr_2O_3 was observed

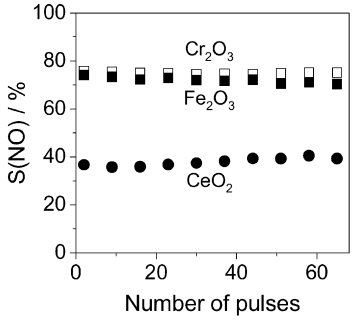

Fig. 8. NO selectivity over the oxides at 1073 K versus the number of pulses in sequential pulsing of O_2:Xe = 1:1 and NH_3:Ne = 1:1 with $\Delta t = 2$ s. Pulse size of O_2 and $NH_3 \sim 10^{16}$ molecules.

only in the first 20 pulses of NH_3, the fraction of lattice oxygen leading to NO was estimated as ca. 5% of the available surface oxygen. This gives a measure of the very low density of active sites in the catalysts leading to the desired product. Different than CeO_2 and Cr_2O_3, the ratio of O_r/O_s over Fe_2O_3 exceeds 1 (Fig. 7), and no H_2 was detected in the NH_3 multipulse experiments (Fig. 6). These observations can be understood considering that more than one monolayer of oxygen can be removed from the iron oxide surface by NH_3, leading to NO and H_2O. Taking these experimental observations into account, the high stability of Fe_2O_3 for NO production in O_2-free ammonia oxidation can be explained by assuming replenishment of active surface lattice oxygen through migration of lattice oxygen from the bulk. Otherwise, the surface of Fe_2O_3 would be fully reduced after ca. 300 pulses of ammonia (Fig. 7), and the relatively high production of NO shown in Fig. 4 and the absence of H_2 could not be accounted for.

3.3. Mars–van Krevelen character of ammonia oxidation

The results shown in Fig. 6 provide evidence that lattice oxygen species of metal oxides efficiently dehydrogenate ammonia, leading to nitric oxide in the absence of gas-phase oxygen. But the production of NO decreases (over Fe_2O_3) and drops to zero (over Cr_2O_3 and CeO_2) due to the stoichiometric reaction of active surface lattice oxygen species to the desired reaction product. As shown in Fig. 8, the NO selectivity can be stabilized if O_2 is supplied to the metal oxide catalysts. Stable NO selectivity values of ca. 40% over CeO_2 and ca. 75% over Cr_2O_3 and Fe_2O_3 were obtained in pump-probe experiments of O_2 and NH_3 using a time delay of 2 s. It is important to emphasize that this time delay was long enough to avoid the simultaneous presence of O_2 and NH_3 in the microreactor; that is, the reduction and reoxidation steps are separated. Based on the foregoing observations, it can be concluded that the high-temperature ammonia oxidation to nitric oxide over oxide-based materials follows a Mars–van Krevelen type scheme (also referred to as a redox or regenerative mechanism) [25]. The characteristic feature of this mechanism is that some products of the reaction leave the solid catalyst's surface with one or more constituents of the catalyst's lattice [26]. This reaction scheme has been regularly considered in (amm)oxidations and oxidative dehydrogenations of C-containing substrates over oxides of reducible metals [25–28]. But this piece of evidence for the ammonia oxidation at high temperature (>1000 K) is novel; no systematic mechanistic study has been dedicated to this industrially relevant reaction over oxide surfaces. According to this reaction scheme, NH_3 is activated by lattice oxygen at the surface (oxidized catalyst), resulting in NO formation and anion vacancies in the oxide lattice (reduced catalyst). The catalytic cycle is closed on reoxidation of the vacancies. Replenishment of the vacancy can be accomplished through dissociative adsorption of gas-phase O_2 or diffusion of bulk oxygen. The original work by Mars and van Krevelen [25] did not explicitly discriminate between these two mechanisms and did not consider the involvement of bulk oxygen diffusion. Multiple pulses of ammonia over the catalysts strongly suggested replenishment of surface anion vacancies by bulk oxygen for Fe_2O_3; however, the participation of bulk oxygen in Cr_2O_3 and CeO_2 was limited and effective vacancy regeneration was achieved only by dissociative adsorption of gas-phase O_2. This result strongly suggests the higher oxygen mobility in iron oxide compared with that in chromium and cerium oxides. But unfortunately, further discussion cannot go forward, because, to the best of our knowledge, no studies tackling the stability and diffusion of oxygen vacancies in metal oxides similar to those studied here have been reported. Studies available in the literature basically involve DFT calculations over nonreducible or barely reducible metal oxides (e.g., MgO, CaO, BaO, α-Al_2O_3, ZnO), concluding with a very high activation barrier for oxygen diffusion and creation of oxygen vacancies [29,30]. The bulk O diffusion for site regeneration can be considered a priori as a very slow step, and thus under realistic conditions (i.e., feed mixture of NH_3 in air), oxygen vacancies can be expected to be reoxidized mainly through dissociative adsorption of gas-phase O_2. Indirect evidence to support this statement can be obtained from the experiments shown in Figs. 6 and 8. In contrast to the NH_3 multipulses shown in Fig. 6, NO selectivity over the oxide catalysts does not depend on the number of NH_3 pulses when O_2 and NH_3 are separated by a relatively long delay of 2 s (Fig. 8). This indicates that active oxygen species are restored in the O_2 pulse. In conclusion, the capability of iron oxide to facilitate oxygen mobility is not expected to produce a better catalyst for NH_3 oxidation to NO in ammonia–oxygen mixtures. However, this property can become highly relevant in a potential process in which oxygen and ammonia are fed separately and periodically or under highly reducing conditions (e.g., in defects of O_2 due to inappropriate mixing of the ammonia–air mixture).

The basic mechanistic difference between the nature of surface oxygen species involved in ammonia oxidation over platinum-group metals (adsorbed O [6–12,22]) and over oxide-based materials (lattice O) can be a reason for the unsuccessful replacement of PGM gauzes by OBM catalysts in industry by using identical reaction conditions for both types of catalysts, because the kinetics likely are governed by different reaction steps. Accordingly, different requirements in terms of operating conditions (i.e., temperature and partial pressure of reactants) are expected for optimal operation over oxide-based catalysts. The unique features of the TAP reactor allowed us to gain mechanistic insight into the high-temperature ammonia oxida-

tion over metal oxides by quantitatively probing active and/or selective oxygen species. We are currently examining whether the rate-determining step of ammonia oxidation over oxides of varying natures is related to the creation of oxygen vacancies by the reaction of NH_3 with lattice oxygen or to the regeneration of the vacancy by dissociative adsorption of gas-phase O_2.

4. Conclusion

We have investigated the mechanism of the high-temperature ammonia oxidation over oxide-based catalysts (CeO_2, Cr_2O_3, and Fe_2O_3) by means of TAP. Our results strongly suggest that the overall scheme of ammonia oxidation is very similar over the oxides and commercial Pt_{95}–Rh_5 gauze. NO is a primary product of NH_3 oxidation, whereas N_2 is formed mainly through consecutive transformations of NO. But the nature of the oxygen species involved in NO production differs significantly over the 2 types of catalysts. Multipulse NH_3 experiments in the absence of gas-phase O_2 demonstrated the participation of surface lattice oxygen in the reaction of NH_3 to NO over metal oxides. The process can be generally described by a Mars–van Krevelen type scheme, in which ammonia is activated by lattice oxygen at the surface leading to NO formation and anion vacancies in the oxide lattice. The replenishment of these vacancies by diffusion of bulk oxygen was clearly evidenced over Fe_2O_3; however, participation of bulk oxygen in Cr_2O_3 and CeO_2 was limited, and vacancy regeneration was effective only by dissociative adsorption of gas-phase O_2. Based on our results, we posit that the capability of certain oxides for ionic conductivity (high O mobility) itself does not lead to a better catalyst for NH_3 oxidation to NO under realistic burner conditions using ammonia–air mixtures.

Acknowledgments

Support was provided by Yara International, the Spanish MEC (project CTQ2006-01562/PPQ), and Consolider-Ingenio 2010 (grant CSD2006-003).

References

[1] R.J. Farrauto, C.H. Bartholomew, Fundamentals of Industrial Catalytic Processes, Chapman & Hall, London, 1997, p. 481.
[2] J. Pérez-Ramírez, F. Kapteijn, K. Schöffel, J.A. Moulijn, Appl. Catal. B 44 (2003) 117.
[3] V.A. Sadykov, L.A. Isupova, I.A. Zolotarskii, L.N. Bobrova, A.S. Noskov, V.N. Parmon, E.A. Brushtein, T.V. Telyatnikova, V.I. Chernyshev, V.V. Lunin, Appl. Catal. A 204 (2000) 59, and references therein.
[4] Y. Wu, T. Yu, B. Dou, C. Wang, X. Xie, Z. Yu, S. Fan, Z. Fan, L. Wang, J. Catal. 120 (1989) 88.
[5] J. Pérez-Ramírez, B. Vigeland, Angew. Chem. Int. Ed. 44 (2005) 1112.
[6] C.W. Nutt, S.W. Karup, Nature 224 (1969) 169.
[7] T. Pignet, L.D. Schmidt, J. Catal. 40 (1975) 212.
[8] J.L. Gland, V.N. Korchak, J. Catal. 53 (1978) 9.
[9] M. Asscher, W.L. Gurthie, T.-H. Lin, G.A. Somorjai, J. Phys. Chem. 88 (1984) 3233.
[10] W.D. Mieher, W. Ho, Surf. Sci. 322 (1995) 151.
[11] J.M. Bradley, A. Hopkinson, D.A. King, J. Phys. Chem. 99 (1995) 17032.
[12] M. Baerns, R. Imbihl, V.A. Kondratenko, R. Kraehnert, W.K. Offermans, R.A. van Santen, A. Scheibe, J. Catal. 232 (2005) 226.
[13] F. Trifirò, I. Pasquon, J. Catal. 12 (1968) 412.
[14] D.W. Griffiths, H.E. Hallam, W.J. Thomas, J. Catal. 17 (1970) 18.
[15] N.I. Il'chenko, G.I. Golodets, J. Catal. 39 (1975) 57.
[16] N.I. Il'chenko, G.I. Golodets, J. Catal. 39 (1975) 73.
[17] O.N. Sil'chenkova, V.N. Korchak, V.A. Matyshak, Kinet. Catal. 43 (2002) 394.
[18] E.M. Slavinskaya, S.A. Veniaminov, P. Notté, A.S. Ivanov, A.I. Boronin, Yu.A. Chesalov, I.A. Polukhina, A.S. Noskov, J. Catal. 222 (2004) 129.
[19] J.T. Gleaves, G.S. Yablonskii, P. Phanawadee, Y. Schuurman, Appl. Catal. A 160 (1997) 55.
[20] J. Pérez-Ramírez, E.V. Kondratenko, Catal. Today 121 (2007) 160.
[21] J. Pérez-Ramírez, E.V. Kondratenko, Chem. Commun. (2004) 376.
[22] J. Pérez-Ramírez, E.V. Kondratenko, V.A. Kondratenko, M. Baerns, J. Catal. 227 (2004) 90.
[23] J. Pérez-Ramírez, E.V. Kondratenko, V.A. Kondratenko, M. Baerns, J. Catal. 229 (2005) 303.
[24] E.V. Kondratenko, J. Pérez-Ramírez, Appl. Catal. A 289 (2005) 97.
[25] P. Mars, D.W. van Krevelen, Chem. Eng. Sci. Spec. Suppl. 3 (1954) 41.
[26] C. Doornkamp, V. Ponec, J. Mol. Catal. A Chem. 162 (2000) 19.
[27] R. Schlögl, A. Knop-Gericke, M. Havecker, U. Wild, D. Frickel, T. Ressler, R.E. Jentoft, J. Wienold, G. Mestl, A. Blume, O. Timpe, Y. Uchida, Top. Catal. 15 (2001) 219.
[28] R.K. Grasselli, Top. Catal. 21 (2002) 79.
[29] J. Carrasco, N. Lopez, F. Illas, Phys. Rev. Lett. 93 (2004) 225502.
[30] J. Carrasco, N. Lopez, F. Illas, H.J. Freund, J. Chem. Phys. 125 (2006) 074711.